Electrocatalytic oxidation and reduction of H_2O_2 on Au single crystals

Ana M[a]. Gómez–Marín[a,b,*], Ana Boronat[a], Juan M. Feliu[a,*]

[a]Instituto de Electroquímica, Universidad de Alicante, Apt 99, E-03080 Alicante, Spain.

[b]Instituto de Química de São Carlos, Universidade de São Paulo, Caixa Postal 780, Dept. Fisico Quimica, *Av. Trabalhador São-Carlense 400, CEP 13566-590,* SP, Brazil.

*Corresponding author. Tel.: +55 16 3373 9945; fax: +55 16 3373 9952. *E-mail address: amgomezma@iqsc.usp.br (A.M. Gómez–Marín).* Tel.: +34 965 909 301; fax: +34 965 903 537. *E-mail address: juan.feliu@ua.es (J.M. Feliu).*

Abstract

In this work, the reduction and oxidation of hydrogen peroxide on Au single crystals is studied in weakly adsorbing electrolytes. Results are discussed in terms of the potential of zero charge and the adsorption strength of different anions, which in turn depend on the crystallographic orientation of the electrode. Close to the reaction onset, both reactions follow the same activity trend with Au(100) and Au(111) being the most and the least active surface planes, respectively. At high potentials, gold oxides inhibit the oxidation of H_2O_2, which seems to be controlled by a surface process.

Keywords: Hydrogen peroxide oxidation, hydrogen peroxide reduction, gold single crystals, rotating disk electrodes, Koutecky-Levich equation, potential of zero charge.

1. Introduction

Among fuel cell cathodic processes, oxygen reduction reaction (ORR) is undoubtedly the most important one, and its slow kinetics is arguably the main bottleneck for the large-scale

commercialization of these devices. Therefore, elucidating the ORR mechanism has been the subject of a large number of works in the last decades, although there are still many kinetics aspects of this reaction that are not fully understood. According to the current state of art, ORR can proceed via either a $4e^-$ or a $2e^-$ pathway. In the first case, water is the final product, well through a direct route [1–11],

$$O_2 + 4H^+ + 4e^- \rightleftarrows 2H_2O \qquad E^0 = 1.229\ V \qquad (1)$$

or through a serial route, producing hydrogen peroxide as intermediate species [1–11],

$$O_2 + 2H^+ + 2e^- \rightleftarrows H_2O_2 \qquad E^0 = 0.695\ V \qquad (2)$$

which can be further reduced to H_2O in a subsequent step, according to [1–11]

$$H_2O_2 + 2H^+ + 2e^- \rightleftarrows 2H_2O \qquad E^0 = 1.763\ V \qquad (3)$$

In the second case, H_2O_2 is the final product. Additionally, H_2O_2 can also disproportionate in a non-electrochemical bimolecular reaction, giving rise to water and oxygen [12],

$$H_2O_2 \rightleftarrows \frac{1}{2}O_2 + H_2O \qquad \Delta G_0 \approx -1.096\ eV \qquad (4)$$

Whereas Pt catalysts undergo almost exclusively the $4e^-$ process [2–11], the selectivity of gold changes between the $4e^-$ and $2e^-$ pathways depending on the experimental conditions and the crystallographic orientation of the Au surface [1,13–25]. Nevertheless, even for Pt electrodes, a serial route involving H_2O_2 as an intermediate specie has been proposed [2,3]. In both cases, however, Tafel slope measurements suggest the first electron transfer as the rate-determining step (RDS) [1–11,13–25], leaving considerable freedom to speculate about the sequence of the following, comparatively fast, steps of the mechanism. Hence, despite decades of research, the exact mechanism of this reaction is still unknown.

One indirect approach to gain insights about the ORR mechanism is through the study of the reaction pathway of its intermediate species on different noble metals, which may give valuable information. This may be particularly important in the case of H_2O_2, considering early studies on polycrystalline metals that highlighted a very complex, interrelated dynamics of the near-reversible O_2/H_2O_2 and H_2O_2/H_2O couples [5,14,26–32]. However, comparatively few reports have been devoted to this subject [5,9,14–18,20,21,24,25,33–40], especially for Au single crystals in acid media. In this case, the hydrogen peroxide oxidation reaction (HPOR), the inverse of Eqn. (2), and hydrogen peroxide reduction reaction (HPRR), Eqn. (3), have been only transversely investigated in ORR studies [14–18,20,21,24], because in these electrodes H_2O_2 is the main ORR final product [1,13–25]. Therefore, in order to fill in this gap, the work reported here attempts to study the reactivity of H_2O_2 on Au single-crystals in acidic media.

The manuscript will be divided in four parts. In the first part, a description of current-potential profiles of Au single crystals in 0.1 M $HClO_4$ (pH = 1.2) and NaF/$HClO_4$ (pH = 4.1), with and without 1 mM of H_2O_2, is given. Later, in the second and third parts, rotating disk electrode experiments for the reduction and oxidation of H_2O_2 reactions (HPROR) are analysed. The manuscript ends with a brief discussion about the inhibiting role of Au oxides on the H_2O_2 oxidation during negative-going scans. Results are discussed in terms of the potential of zero charge and surface adsorption of weakly adsorbing anions, which in turn depend on the crystallographic orientation of the electrode.

2. Experimental

Gold single-crystal electrodes were made of small (ca. 2 mm diameter) single-crystal beads, obtained by melting a 0.5 mm Au wire (99.999%, Goodfellow). After careful cooling, the resulting single-crystal beads were oriented, cut and polished following the procedure

described for Pt [41–43]. All the experiments were carried out in a two–compartment, three-electrode all-glass cell, following a well-detailed experimental protocol [43]. Prior to each experiment, the electrodes were flame annealed, cooled in a hydrogen/argon atmosphere and transferred to the cell protected by a drop of ultra–pure water saturated with these gases. All potentials were measured against the Reversible Hydrogen Electrode (RHE) and a large Au wire coil was used as a counter electrode. Incidentally, in some cases a flame annealed Pt counter-electrode was also used, without observing any difference. This could suggest that the reactions involved are not so affected by the presence of tiny amounts of isolated Pt atoms as those involved in hydrogen oxidation and reduction reactions.

All voltammetric scans were collected at freshly annealed surfaces, cycled first in the low potential region to verify their quality as well as the cleanliness of the surface. The stability of the voltammetric profiles with time was carefully checked to ensure solution cleanliness.

Two types of solutions with the least adsorbing anions were employed during experiments: 0.1 M $HClO_4$, pH = 1.2, and 0.1 M NaF/$HClO_4$, pH = 4.1, in ultrapure water (Purelab Ultra, Elga–Vivendi). In the last case, the experimental conditions were defined to avoid local pH changes at the interphase by employing a buffered solution for pH = 4.1. This solution was prepared by adding perchloric acid (Merck, suprapur) in an appropriate amount to a 0.1 M solution of sodium fluoride (Merck, suprapur) [44], which allows the study of solutions at this pH without the interference of strong specific adsorption of anions on gold surfaces [45–49]. The use of NaF instead of $KClO_4$ avoids the purification of $KClO_4$ by recrystallization, required for removing impurities present on it. Additionally, previous studies with NaF/HF buffered solutions required the use of relatively high concentration of HF acid, hampering the achievement of the high cleanliness degree required when working with single crystals [44,50,51].

Rotating disk electrode (RDE) experiments were performed by using a hanging meniscus rotating disk electrode (HMRDE) configuration [52]. For this purpose, an electrode holder for bead–type single crystal electrodes was adapted to a Radiometer EDI–10K rotor. The electrode was placed in the holder in such a way that its surface was perpendicular and centered to the rotation axis (as much as possible). With this arrangement, the higher rotation speed that can be achieved, without breaking meniscus, is ~4000 rpm [11].

3. Results and discussion

Before analyzing the current-potential profiles in hydrogen peroxide-containing solutions, it is important to describe the electrochemical processes in the solutions without H_2O_2. Figure 1 shows typical cyclic voltammograms (CVs) of Au(111), Au(100) and Au(110) electrodes in Ar-saturated, 0.1 M $HClO_4$, pH = 1.2, and 0.1 M NaF/$HClO_4$, pH = 4.1 at 0.05 V s^{-1} from 0.06 to 1.7 V (main figure) and from 0.06 to 1.2 V (Inset). Current profiles in Fig. 1 agree well with previously published curves [22,45,53], confirming the high quality of the gold surfaces employed in this study. As reported before [45,53], CVs are characteristic for a given crystal structure, especially at higher potentials, E > 1.2 V, and depict characteristic features that allow identifying distinct potential regions.

In the positive-going scan, small anodic currents at low potentials correspond to capacitive charging of the electrical double layer. From ~0.3 to 1.2 V, anion adsorption, accompanied by partial discharge of water molecules of their hydration shells, takes place, and its extent depends on the symmetry of surface sites: Au(111) > Au(110) > Au(100) [54]. Anions seem to be fully discharged on (111) and (110) planes, but little or not at all on (100) plane [54], and this governs the magnitude of the charge transfer of OH deposition in between adsorbed anions: Au(110) > Au(100) > Au(111) [54]. For the (100) and (111) planes, the lifting of the surface reconstruction, induced because of the flame annealing from Au(100)-

(5x20) to Au(100)-(1x1) and Au(111)-(1x23) to Au(111)-(1x1), also occurs in this region, at ~0.86 V and ~0.72 V in 0.1 M $HClO_4$, respectively [55]. These peaks are sharper in the first cycle after the flame annealing, but become smaller upon cycling because of the slow kinetics of the reconstruction process at potentials negative to the pzc [22,55].

Surface oxidation starts at E > 1.2 V, at a less positive potential for the surfaces with weaker specific anion adsorption [53,54,56,57]. At higher potentials, the place exchange/turnover processes occur, as the RDS [54,57–59], and leads to a surface roughening at an atomic scale [53,54,57,59–63]. It constitutes the initial stage of phase oxide growth and is determined by the strength of anion adsorption, being the most difficult on the {111} and the easiest on the {100} plane [54], although it occurs in greater extent in the presence of stronger specifically adsorbed anions [58,59]. This process is quite fast [54] and takes place when the gold surface oxide is formed at low coverage, approximately once a charge of ~100 μC cm^{-2} has been transferred to the electrode [57], ~E ≥ 1.40 V on Au(111) [60], by a complex surface reaction mechanism [54,57,63].

Reversing the scan direction results in a rapid cessation of oxidation currents, followed by a number of negative peaks, between one and three, depending on the orientation plane, the upper limit potential of the positive-going scan, the sweep rate, the pH and temperature of the solution [45,54,57,63], Fig. 1. These cathodic peaks have been attributed to the reduction of three different oxidized gold compounds existing all together at the electrode surface [57,63], Au^{+1}, Au^{+2} and Au^{+3}. An essentially similar reduction pattern for polycrystalline gold, (poly)-Au, may suggest that the structure of these oxides is almost independent of the substrate orientation [54]. The rough surface morphology remains almost unaltered until the onset of the main reduction peak, pointing to stability of the place-exchanged gold oxide in the potential region of the negative scan before the reduction [60].

In the RHE scale, increasing the solution pH from 1.2 to 4.1 should shift 0.17 V the potential of anion-related peaks, because of the nature of the reference electrode [64], and slightly modify the oxide growth processes for Au single crystals [54,65]. However, if the anion interaction strength with the surface simultaneously changes with the solution pH, different shifts in potential are expected. Stronger anion adsorption, or higher anion concentration, shifts anion adsorption and OH/O adsorption peaks toward lower and higher potentials, respectively. Therefore, the current increase and the positive shift in peaks' potentials, lower than 0.17 V, in the double layer for all planes, and the slight increase in the first oxidation peak on Au(110) and Au(100) in Fig. 1 can be ascribed to the "stronger" interaction of F^-, relative to ClO_4^-, with the surface [45–47]. This is because, in our case, the concentration of electrolyte anions can be considered approximately the same for both pHs.

Changes from pH 1.2 to 4.1 in Fig. 1 are larger for Au(110) and smaller for Au(111) planes, especially in the oxide growth region. Interestingly, in this latter plane, even an advance in the first oxidation peak is seen. This result can be attributed to the larger strength of the hydrogen bond network between F^- anions and water molecules, relative to ClO_4^- [66], giving rise to a larger net orientation of the water molecules [67], that modifies the first stage of surface oxide formation [68]. This is because, as stated before [54,59], specifically adsorbed anions on Au(111) not only hinder the oxidation of the electrode but also provide an alternative reaction path, at less positive potentials than the main reaction in the oxidation process, for the discharge of H_2O hydrogen bonded to the anions.

3.1.1. Influence of hydrogen peroxide in the current-potential response of Au single crystals

Once the processes in blank solutions have been analyzed, changes in voltammograms in H_2O_2-containing solutions will be described. Figure 2 shows CVs in 0.1 M perchloric acid + 1 mM H_2O_2 for all low index planes from 0.06 to 1.7 V. For the sake of comparison, CVs for the basal planes are superimposed in Fig. 2D. Blank CVs for each crystallographic orientation are also given, from 0.06 to 1.2 V (multiplied by 10) and from 0.8 to 1.7 V (vertically displaced) in order to facilitate the analysis of the changes in the oxide formation region. As it can be seen in Fig. 2, both reactions, the HPRR and HPOR, are structure sensitive reactions, especially in the first case, for which the reaction only occurs at high overpotentials, Eqn. (3).

In the negative-going scan, the HPRR begins at ca. E < 0.5, 0.6 and 0.7 V for Au(111), Au(110) and Au(100), respectively, in a potential region where the electrode surface is already covered by adsorbed anions from the electrolyte, and OH deposition barely takes place, Fig. 1. The activity trend close to the reaction onset is Au(100) > Au (110) > Au(111), following the inverse tendency of the anion adsorption strength: Au(111) > Au (110) > Au(100). At lower potentials, however, the activity order changes to Au(110) > Au (100) > Au(111), and now follows the increase in the potential of zero charge (pzc) of the electrodes 0.27 Au(110) < 0.46 Au (100) < 0.58 V Au(111) [17,22,47–49,55]. These findings suggest that H_2O_2, or an intermediate product during the HPRR, have to compete with adsorbed anions for Au surface sites, and the reduction can only take place once adsorbed OH is not stable on the surface, which in turn depends on the surface electrode structure. Therefore, the charge on the electrode and the magnitude of anion adsorption would determine the reactivity of Au single crystals for the HPRR.

The appearance of positive currents in the CVs takes place at E > 0.75, 0.78 and 0.82 V for Au(100) < Au (110) < Au(111), respectively, in a potential region where OH adsorption from the partial discharge of water molecules of anions hydration shells just begins, Fig. 1. In contrast to the HPRR, the HPOR occurs closer to the standard potential of the reaction, Eqn. (2), and diffusion-limiting currents are quickly reached, even before the surface oxidation process in blank voltammograms takes place, Fig. 1. Nevertheless, both reactions, HPRR and HPOR, follow the same activity order regarding the reaction onset, highlighting the role of the anion adsorption in the reactivity of Au single crystals. Similar activity trend is also registered for the reduction of oxygen, produced during the HPOR at high potentials, in the negative-going scan, Fig. 2D, in agreement to what has been reported before [20], although in H_2O_2-containing solutions the system O_2/H_2O_2 behaves more "reversible" and ORR currents are higher than in O_2-saturated, H_2O_2-free, solutions [14,25].

At high enough overpotentials, E > 1.2 V, the oxidation of the surface begins, parallel to H_2O_2 oxidation, with subtle, but measurable, changes in the CV, as depicted in Fig. 2. From this figure, a small increase in the first oxidation peak, besides to a small shift to higher potentials, is evident for all Au planes, while the other processes practically appear at the same potentials. This first peak has been identified as the beginning of surface oxidation by OH deposition from bulk water in parallel with anion desorption [45,53,57,63]. Close to 1.7 V and during the negative-going scan, in a potential region where surface reordering is taking place although no significant current is being passed to the electrode surface in blank voltammograms, Fig. 1, oxidation currents sharply decrease. The oxidation increases again only after the main reduction process occurs, but does not reach the same measured current in the positive-going scan. The decrease and the recovery in the oxidation currents occurs first on Au(110) and last on Au(111).

Initial studies on the catalytic decomposition of H_2O_2 on (poly)-Au suggested that, because H_2O_2 easily reduces $Au(OH)_3$, this process necessarily involves the intervention of oxides formed on the electrode surface [12] and thus, analogously, it was also proposed that the HPOR on Au occurs by an indirect process through an adsorbed Au-oxide [15,28,34], such as:

$$AuO_{ads} + H_2O_2 \rightleftarrows Au + H_2O + O_2 \qquad (5)$$

which is first-order regarding the H_2O_2 concentration. In this sense, the oxide can react with H_2O_2 only if the potential of the cathodic reduction of the oxide is more positive than the potential of the anodic oxidation of H_2O_2, Eqn. (2) [12], as in the case of gold electrodes. However, the fact that the HPOR only takes place once the discharge of water molecules, from anion hydration shells, can occur in H_2O_2-free solutions, Fig. 1, suggest that, instead of adsorbed oxygen, the reacting species with H_2O_2 would be the adsorbed OH [28]:

$$2AuOH_{ads} + H_2O_2 \rightleftarrows 2Au + 2H_2O + O_2 \qquad (6)$$

In this mechanism, the oxidation current in the CVs comes from the re-oxidation of the electrode surface, similar to what has been suggested for the HPOR on Pt surfaces [12,33,35,36,38,39]. At higher potentials, it has been proposed that the oxidation of H_2O_2 would be hindered because the reactivity of bulk Au oxide is lower than the reactivity of adsorbed oxide [15,34].

3.1.2. Hydrogen peroxide reduction

Rotating disk measurements allow determining kinetic parameters of electrode reactions [64]. Figure 3 resumes polarization curves for HORR on Au(111), Au(110) and Au(100) at 400, 900, 1600 and 2500 rpm in, Ar-saturated, 0.1 M $HClO_4$, pH = 1.2, and 0.1 M $NaF/HClO_4$, pH = 4.1, + 1 mM H_2O_2 solutions. As it is observed, reduction currents at the

lowest pH are almost under reaction control, *i.e.* practically independent of the rotation rate, ω, while they increase for all crystallographic planes and become slightly ω-dependent with an increase in the solution pH, despite of the greater extent of anion adsorption at 0.1 M NaF/$HClO_4$, Fig. 1. Nevertheless, in both solutions the same activity trend is found: Au(100) > Au(110) > Au(111) close to the reaction onset, and Au(110) > Au(100) > Au(111) at lower potentials.

For a first order reaction with respect to the reactant, as suggested for the HPRR on (poly)-Au [15,34], the measured current density in RDE experiments, j, can be expressed as a linear combination of the kinetic current density that would have been obtained in absence of mass transport, j_k, and the diffusion limiting current density through the solution boundary layer, j_{lim}. This is represented by the Koutecky-Levich equation [11,64]:

$$\frac{1}{j} = \frac{1}{j_k} + \frac{1}{j_{lim}} \qquad (7)$$

considering the Levich expression for the diffusion limiting current [11,64]:

$$j_{lim} = 0.62nFD_0^{2/3}\upsilon^{-1/6}\omega^{1/2}C_o^* \qquad (8)$$

where n is the number of transferred electrons, F the Faraday's constant, D_0, v and C_0^* are the diffusion coefficient, the kinematic viscosity and the concentration of hydrogen peroxide in the electrolyte and ω is the electrode rotation rate. From this set of equations, the kinetic current density, j_k can be calculated from the intercept of the plot of j^{-1} vs. $\omega^{-½}$ at different potentials if these plots yield straight lines and are parallel to each other. In our case, these requirements are well full filled for Au(110) in both solutions, for Au(100) in 0.1 M $HClO_4$ and for Au(111) in 0.1 M NaF/$HClO_4$ in the whole potential interval where the reduction takes place. For Au(100) 0.1 M NaF/$HClO_4$ and Au(111) in 0.1 M $HClO_4$, these conditions only are found for E < 0.36 V and E > 0.5 V.

Similar tendencies are also calculated for all basal planes if instead of the plot of j^{-1} vs. $\omega^{-½}$, suitable for reactions with a reaction order, *m*, of one [16–20,64,69], a plot of j^{-2} vs. $j^{-1}\omega^{-½}$ at different potentials is employed, appropriate for reactions with a *m* of one-half (0.5) [16–20,69], derived from

$$\frac{1}{j^2} = \frac{1}{(j_k)^2} + \frac{1}{j j_{lim}} \qquad (9)$$

This result indicates a lack of sensitivity of Eqns. (7) and (9) to the reaction order for HPRR on Au single crystals, which probably reflects the strong coupling between the number of electrons exchanged in the reaction and the overall reaction order, inherent to rotating disk experiments, as highlighted long time ago for reactions with complex mechanisms [69]. In these cases, it has been recommended better to employ the following equation developed for a totally irreversible reaction [16,69],

$$j = k[\mathrm{HO_2^-}]^m[\frac{j_{lim}-j}{j_{lim}}]^m \qquad (10)$$

where *k* is the reaction rate constant and $[H_2O_2]$ is the bulk concentration of H_2O_2 in solution [16]. In addition, considering that [69]

$$j_k = k[\mathrm{HO_2^-}]^m \qquad (11)$$

Therefore, by plotting log (*j*) *vs.* log $[\frac{j_{lim}-j}{j_{lim}}]$ at different rotation rates and constant potential, the reaction order can be calculated, without knowing the number of transferred electrons. Figure 4 resumes the log (j_k) for all Au single crystals in both solutions. Curves were calculated by employing Eqn. (10) with a j_{lim} value equal to j_{lim} for HPOR, although exact results are obtained from Eqns. (7) (dashed lines) and (9), which reveals the complex dynamics for the HPRR on Au electrodes. Indeed, only at the most negative potentials a constant value of m is determined from Eqn. (10), although different for each single crystal

and medium, despite the good linear correlations. In addition, from curves in Fig. 4, an apparent shift in reduction currents toward positive potentials at increasing pH is seen. This shift is ~180 (140), ~150 (120) and ~115 (30) mV for Au(110), Au(111) and Au(100) at lower (higher) potentials, respectively.

From Fig. 4, Tafel slopes from 295 to 380 mV are calculated for Au(110) and Au(100) in NaF/$HClO_4$, respectively. Similarly, for all Au single crystals Tafel slopes lower than ~ 30 mV of these values are obtained in 0.1 M $HClO_4$ solutions. In this latter electrolyte, an even higher Tafel slope of ~500 mV is measured for Au(100) at E < 0.36 V, when its activity toward the HPRR becomes lower than the activity on Au(110), as mentioned above. These high Tafel slopes indicates a weak potential-dependence of j_k for all electrodes, suggesting that either the RDS is an initial one-electron step with a relatively high coverage of adsorbed reactants or products [7,18], or the RDS, and any step preceding it, is a chemical step, and not an electrochemical reaction [16,17]. If this is the case, the small variation of the rate constant with potential may be originated from secondary changes due to the potential dependence of the state of adsorption of anions and other features of the surface [16].

Cyclic voltammograms at fast scan rates for Au(111) in H_2O_2-containing 0.1 M $HClO_4$ solutions (not shown) are not different to CVs in absence of peroxide [45] and thus, they do not reveal the presence of any adsorbed species coming from H_2O_2. Therefore, it is more likely that the RDS in the HPRR would be a chemical reaction. In this sense, first studies on HPRR on (poly)-Au electrodes suggested a mechanism involving a H_2O_2 dismutation, giving rise to radical species [15,34]

$$2H_2O_2 \rightarrow HO_2 + OH + H_2O \qquad (12)$$

along with

$$H_2O_2 \rightarrow 2AuOH_{ads} \qquad (13)$$

According to this mechanism, the electrode surface may be saturated by OH and HO_2 radicals and the reaction would become independent of the H_2O_2 concentration. A similar mechanism involving Eqn. (13) has also been proposed for the HPRR on Pt [36,39,38], in which case the production of OH radicals in H_2O_2 containing solutions have been recently reported [70], giving support to the occurrence of Eqn. (13). Under this scheme, the measured reduction current would indirectly come from

$$AuOH_{ads} + H^+ + e^- \rightleftarrows Au + H_2O \qquad (14)$$

Therefore, the higher pH-dependence of Au(110) and Au(111) for the HPRR, relative to Au(100), may be explained by considering the H_2O_2 adsorption strength on Au single crystals: Au(110) > Au(111) > Au(100) [71], together with the shift to higher potentials in the pzc in the RHE scale. This change decreases the amount of adsorbed anions on the surface at a given potential, liberating Au sites, available now for other weaker adsorbing species. Indeed, under this view, a decrease on the influence of the potential on j_k would be expected, as it is experimentally reflected in the increase in 30 mV in the Tafel slope. For Au(100) the shift is lower because of the lower (and higher) amount of anion (OH) already adsorbed on the surface in 0.1 M $HClO_4$. In these cases, a role of the surface reconstruction is not considered because of the slowness of this transition and the retarding effect of HO_2^- anions on its formation [21].

Strong competition between OH and anions for Au sites and the formation of radicals may give rise to the complex mechanism of the HPRR. However, if the positive potential shift is extrapolated to alkaline solutions, the reduction of H_2O_2 should occur at higher potentials, and to a larger extent, than the one it actually occurs under our conditions [16–18,20,21], which cannot be explained just by considering the competition between OH and anions, as

suggested before [23]. In this latter case, only on Au(111) electrodes reduction currents and Tafel slopes are similar to those found in 0.1 M $HClO_4$. In the other planes, in contrast, reduction currents are slightly higher on Au(110) and significantly greater on Au(100), but not as expected from the pH change reported here, suggesting the presence of other phenomena not accounted in acid solutions.

3.1.3. Hydrogen peroxide oxidation

Rotating disk measurements for the hydrogen peroxide oxidation in Ar-saturated, 0.1 M $HClO_4$, pH = 1.2, and 0.1 M NaF/$HClO_4$, pH = 4.1, + 1 mM H_2O_2 solutions on Au single crystals, from 0.7 to 1.2 V at 400, 900, 1600 and 2500 rpm are given in Figure 5. In contrast to the voltammetric response for the HPRR, oxidation currents in Fig. 5 strongly depend on the electrode rotation rate and, at high potentials, limiting diffusion currents are always reached. Additionally, curves slightly shift at increasing pH but the direction and magnitude of this shift depends on the electrode crystallographic orientation. Moreover, a hysteresis between positive- and negative-going scans is recorded in both electrolytes, but especially at pH 4.1, for all basal planes, and its magnitude is also a function of the rotation rate, being greater at faster ω. Nevertheless, the activity trend among the electrodes is always the same Au(100) > Au (110) > Au(111), regardless the solution and/or the potential range.

Currents in Fig. 5 rapidly increase after the reaction onset but reach a limiting plateau at increasing potentials, especially in 0.1 M NaF/$HClO_4$ in which case limiting diffusion currents are always smaller than in 0.1 M $HClO_4$. Analogous to the HPRR, kinetic analyses for the HPOR were performed by employing Eqns. (7), (9) and (10), and similar correlations were calculated in all cases: negative close to the reaction onset but positive at higher potentials, suggesting a complex mechanism also for this reaction. Indeed, despite good

linear fittings, only at values of potential relatively close to j_{lim}, plotted lines become parallel and, from a plot of log (j) *vs.* log $[\frac{j_{lim}-j}{j_{lim}}]$ at different rotation rates and constant potential, it is possible to determine a rather constant value for the reaction order, Figure 6, which makes difficult to obtain accurate values for *m*.

From Fig. 6, only for Au(111) in 0.1 M $HClO_4$ an *m* value between 0.58 to 0.7 is calculated. In the other cases, *m* values ca. 0.2 to 0.4 are estimated, suggesting an apparent weak dependence of the HPOR on the H_2O_2 concentration. Indeed, at lower potentials than those depicted in Fig. 6, non-constant, smaller values are estimated for *m*, regardless the electrode or the working solution. Similarly, in alkaline media, a rather constant reaction order has been also reported only at high potentials, but equal to 0.5 for the Au(100) [17] and Au(110) [18] surfaces and to 0.35 for the Au(111) plane [18]. However, in contrast to results given here, close to the reaction onset, *m* values increases at decreasing potentials, which was explained because of the heterogeneous decomposition of HO_2^- and the parallel reduction of O_2 formed by the HPOR [16,18].

Nevertheless, as reported for the HPRR above, similar values for j_k are calculated by any of the mathematical approaches, Figure 7, well by employing Eqn. (7) for first order reactions, Eqn. (9) for one-half order reactions, or Eqn. (10) for a generic calculation, regardless the reaction order. From these curves, two Tafel slopes can be considered for almost all cases, being always smaller in the potential range closer to the reaction onset than to j_{lim} and in 0.1 M $HClO_4$ relative to NaF/$HClO_4$ solutions. For Au(111), increasing the pH improves the catalytic activity and Tafel slopes of 63 (121) and 79 (164) mV are calculated at small (large) overpotentials in $HClO_4$ and NaF/$HClO_4$ respectively. In contrast, for Au(110) and Au(100) the oxidation currents increase with pH only at the foot of the oxidation wave, with Tafel slopes of 47 (70) and 43 (60) mV in $HClO_4$ (NaF/$HClO_4$) but they are smaller at

high potentials. In this latter case, Tafel slopes of 120 (and higher than 195) mV are calculated in $HClO_4$ (NaF/$HClO_4$).

The fact that increasing the pH improves the HPOR reactivity of the Au(111) plane, the only plane for which the oxidation process in H_2O_2-free solutions is also positively shifted at increasing pH, Fig. 1, gives an additional support for an indirect mechanism for the HPOR on gold surfaces through adsorbed OH, Eqn. (6). However, the small Tafel slopes close to the reaction onset and the apparent independence on the H_2O_2 concentration of the HPOR not only indicate that Eqn. (6) is not the RDS in the mechanism at low overpotentials, but also do not support a direct oxidation of H_2O_2 on the electrode surface, as suggested in early works with (poly)-Pt [5]

$$(H_2O_2)_{ads} \rightarrow (HO_2^-)_{ads} + H^+ + e^- \qquad (15)$$

In the same framework, Tafel slope data do not support a mechanistic scheme as the one suggested for (poly)-Au [16] and Au single crystals in alkaline solutions [17,18], given by

$$O_2 + e^- \rightarrow AuO_2^-{}_{ads} \qquad (16)$$

$$2O_2^-{}_{ads} + H_2O \rightleftarrows HO_2^- + O_2 + OH^- \qquad (17)$$

Instead, it can be proposed that the OH adsorption, Eqn. (14), from the partial discharge of water molecules of anions hydration shells, is the controlling kinetics in the HPOR mechanism at low overpotentials. Apparent Tafel slopes of 57 (74), 29 (40) and 31 (24) mV calculated at the beginning of the oxide formation in H_2O_2-free $HClO_4$ (NaF/$HClO_4$) for Au(111), Au(110) and Au(100), respectively, Fig. 1, closer to Tafel slopes calculated from Fig. 7, would support this possibility. At higher potentials, however, the increased coverage of adsorbed anions, adsorbed OH or even the structure and orientation of water molecules close to the electrode surface layer [72,73], may hinder the approach of H_2O_2 molecules

and hence, slow down the reaction rate of H_2O_2 and OH_{ads}, Eqn. (6), which may become the RDS in the mechanism. Thus, a weak dependence on the H_2O_2 concentration and high Tafel slopes should be measured, especially in stronger adsorbing electrolytes, as experimentally found from Figs. 6 and 7.

This mechanism is similar to what has been proposed for the HPOR in acid media on (poly)-Au [14,33], in which case Tafel slopes of 77 mV close to the reaction onset [14], and to 120 mV at potentials higher than 1.0 V [15] have been reported. Therefore, as for the HPRR, the dependence of the electrode activity on the crystallographic orientation is only given by differences on anion and OH adsorption on each plane, which in turn would determine the dominant interaction between the H_2O_2 molecule and the electrode surface through Eqn. (6) or Eqn. (13). The question now is how this interaction influences the ORR dynamics, taking into account that the addition of peroxide to O_2-saturated solutions increase the ORR reduction currents [14,25]. This can be understood by considering that the RDS for the ORR under the studied conditions is the first electron transfer given by [13,14,20]

$$\mathrm{AuO_2}_{\mathrm{ads}} + \mathrm{e^-} \rightleftarrows \mathrm{AuO_2^-}_{\mathrm{ads}} \qquad (18)$$

because the surface is assumed to be saturated with species coming from $O_{2,ads}$ [14]. Hence, the addition of H_2O_2 to O_2-saturated solutions improves the ORR activity because, in the potential region in which ORR occurs, the interaction of H_2O_2 with the surface is given by Eqn. (6) and thus, H_2O_2 releases Au surface sites, increasing the number of free Au sites available for the ORR.

3.1.4. Effect of gold oxides in the oxidation of hydrogen peroxide

As described above, after potential excursions at high potentials, E > 1.2 V, there is a clear inhibition in the HPOR during the negative-going scan, Fig. 2. In order to confirm this

finding, rotating disk measurements were also performed until 1.7 V and results are given in Figure 8. It is seen that, parallel to the HPOR, the surface oxidation processes of each basal plane take place and, during the negative-going scan, a decrease in oxidation currents appears in both solutions, 0.1 M $HClO_4$ and NaF/$HClO_4$, reaching a minimum value similar for all cases, practically regardless ω, just before the reduction of gold oxides initiates. This fact strongly suggest that this decrease in current occurs because in this potential region the RDS is a surface process. A similar curve depicting an inhibition in the HPOR because of gold oxides was also reported for Au(311) in alkaline media [19], suggesting that this inhibition takes place regardless the solution pH, however, its possible origin has not discussed so far.

Furthermore, from Fig. 8 it is also clear that for NaF/$HClO_4$ solutions, at faster rotation rates, some CVs in the positive-going scan also depict a decrease in current. This decrease appears once the first monolayer of adsorbed O-containing species has been completed [45], and its magnitude depends on the crystallographic orientation of the electrode: Au(110) > Au(100) > Au(111), although the current almost recovers at higher potentials. This decrease in current is similar to what has also been reported for Pt(111) in H_2O_2-containing solutions [38.74], and it has been attributed to the competence for surface sites between surface oxidation species and HPOR intermediate species, reflecting the heterogeneous nature of the electrode surface in this potential region [53,54,57,59–63].

It is probable that the decrease in current in the negative going scan appears because of the different reactivity of the several Au oxidized species present in the electrode surface with H_2O_2 after the surface oxidation arises. As described above, in this potential region, besides the replacement of adsorbed anions by adsorbed OH, the place exchange process occurs and at least three oxidized gold compounds, with different formation rate, could exist simultaneously at the electrode surface [57,63]. It is then probable that H_2O_2 could react

with more than one species, reducing them in a chemical reaction, while only those reduced gold atoms that oxidize again would transfer electrons to the electrode surface, contributing to the measured current.

Moreover, the formation and the successive reduction of the gold oxide modify the initial surface structure, and new sites are created, more or less favorable to oxidation and/or reaction with H_2O_2. Indeed, because the formation of new sites is directly dependent on the upper potential limit of the scan, the scan rate, the surface "history", among others, it is found that the inhibition in the HPOR also depends on these factors, Figure 9 [57,63]. In this sense, slower scan rates shift the HPOR curve toward positive potentials, Fig. 9, reflecting the role of anion adsorption and the structure and orientation of water molecules that create stable structures close to the electrode surface [72,73], which may hinder the interaction of H_2O_2 with the electrode surface.

Similarly, the dependence of the HPOR becomes also evident in Fig. 9, where different HPROR curves are shown for two different upper limit potentials, E_{up}, lower than the potential in which surface oxidation takes place, but after several cycles to 1.7 V have been performed. As it can be seen, while curves in the positive-going scan practically superimpose, the current response in the negative-going scan shifts to positive potentials the higher E_{up}. Therefore, under these conditions, the surface state depends on the "history" of the surface and the E_{up}. This "sensibility" of the electrode response for the HPOR, but not the HPRR, is greater for Au(110) and smaller for Au(111), and maybe related to the atomic density of these surfaces, being lower for Au(110) and higher for Au(111) [54], as a stronger adsorption is expected with increasing atomic density at the surface [47].

4. Conclusions

In this work, the interaction of Au single crystals with hydrogen peroxide was studied in acid media. Results were analyzed in light of of the potential of zero charge and the adsorption strength of different anions, which in turn depend on the crystallographic orientation of the electrode. Close to the reaction onset, the activity trend for the hydrogen peroxide reduction reaction (HPRR) and the hydrogen peroxide oxidation reaction (HPOR) is the same with Au(100) and Au(111) being the most and the least active surface planes, but at lower potentials the Au(110) electrode is the best for the HPRR. However, the current response for the HPOR strongly depends on the upper potential limit of the scan, the scan rate and the surface "history" of the electrode. At high potentials, gold oxides inhibit the oxidation of H_2O_2, possibly because of differences in reactivity between the several surface species on the electrode with H_2O_2 and their oxidation reaction. It is proposed that the addition of H_2O_2 to O_2-saturated solutions increases the ORR reduction currents because of an increase in the number of free metallic sites available for the ORR.

Acknowledgments

Support from the Spanish MINECO though project CTQ2016-76221-P (FEDER) and GV through PROMETEOII/2014/013 (FEDER) are greatly acknowledged

References

1. Wroblowa, H., Pan, Y.C., and Razumney, J., *J. Electroanal. Chem.*, 1976, vol. 69, p. 195.

2. Schneider, A., Colmenares, L., Seidel, Y.E., Jusys, Z., Wickman, B., Kasemo, B., and Behm, R.J., *Phys. Chem. Chem. Phys.*, 2008, vol. 10, p. 1931.

3. Seidel, Y. E., Schneider, A., Jusys, Z., Wickman, B., Kasemo B., and Behm, R.J., *Faraday Discuss.*, 2008, vol. 140 p. 167.

4. Hoare, J.P., *J. Electrochem. Soc.*, 1965, vol. 112, p. 602.

5. Hoare, J.P., *J. Electrochem. Soc.*, 1965, vol. 112, p. 608.

6. Urbach, H.B., and Bowen, R.J., *Electrochim. Acta*, 1969, vol. 14, p. 927.

7. Huang, J.C., Sen, R.K., and Yeager, E., *J. Electrochem. Soc.*, 1979, vol. 126, p. 786.

8. Markovic, N.M., Gasteiger, H.A., and Ross, P.N., *J. Phys. Chem.*, 1995, vol. 99, p. 3411.

9. Markovic, N.M., Gasteiger, H.A., and Ross, P.N., *J. Phys. Chem.*, 1996, vol. 100, p. 6715.

10. Grgur, B.N., Markovic, N.M., and Ross, P.N., *Can. J. Chem.*, 1997, vol. 75, p. 1465.

11. Maciá, M.D., Campiña, J.M., Herrero, E., and Feliu, J.M., *J. Electroanal. Chem.*, 2004, vol. 564, p. 141.

12. Bianchi, G., Mazza, F., and Mussini, T., *Electrochim. Acta*, 1962, vol. 7, p. 457.

13. Hoare, J.P., *Electrochim. Acta*, 1966, vol. 11, p. 311.

14. Hoare, J.P., *Electrochim. Acta*, 1966, vol. 11, p. 549.

15. Bianchi, G., Mazza, F., and Mussini, T., *Electrochim. Acta*, 1966, vol. 11, p. 1509.

16. Zurilla, R.W., Sen, R.K., and Yeager, E., *J. Electrochem. Soc.*, 1978, vol. 125, p. 1103.

17. Adzic, R.R., Markovic, N.M., and Vesovic, V.B., *J. Electroanal. Chem.*, 1984, vol. 165, p. 105.

18. Markovic, N.M., Adzic, R.R., and Vesovic, V.B., *J. Electroanal. Chem.*, 1984, vol. 165, p. 121.

19. Anastasijevic, N.A., Strbac, S., and Adzic, R.R., *J. Electroanal. Chem.*, 1988, vol. 240, p. 239.

20. Adzic, R.R., Strbac, S., and Anastasijevic, N., *Mater. Chem. Phys.*, 1989, vol. 22, p. 349.

21. Markovic, N.M., Tidewell, I.M., and Ross, P.N., *Langmuir*, 1994, vol. 10, p. 1.

22. Prieto, A., Hernández, J., Herrero, E., and Feliu, J.M., *J. Solid State Electrochem.*, 2003, vol. 7, p. 599.

23. Blizanac, B.B., Lucas, C.A., Gallagher, M.E., Arenz, M., Ross, P.N., and Markovic, N.M., *J. Phys. Chem. B*, 2004, vol. 108, p. 625.

24. Jirkovsky, J.S., Halasa, M., and Schiffrin, D.J., *Phys. Chem. Chem. Phys.*, 2010, vol. 12, p. 8042.

25. Zheng, Y.L., Mei, D., Chen, Y.-X., and Ye, S., *Electrochem. Commun.*, 2014, vol. 39, p. 19.

26. Kolthoff, I.M., and Jordan, J., *J. Am. Chem. Soc.*, 1952, vol. 74, p. 570.

27. Kolthoff, I.M., and Jordan, J., *J. Am. Chem. Soc.*, 1952, vol. 74, p. 4801.

28. Bockris, J.O.M., and Oldfield, L.F., *Trans. Faraday Soc.*, 1955, vol. 51, p. 249.

29. Bowen, R.J., and Urbach, H.B., *J. Chem. Phys.*, 1968, vol. 49, p. 1206.

30. Hoare, J.P., *J. Electrochem. Soc.*, 1963, vol. 110, p. 245.

31. Hoare, J.P., *Electrochim. Acta*, 1966, vol. 11, p. 203.

32. Wroblowa, H., Rao, M.L.B., Damjanovic, A., and Bockris, J.O.M., *J. Electroanal. Chem. Interfacial Electrochem.*, 1967, vol. 15, p. 139.

33. Hickling, A., and Wilson, W.H., *J. Electrochem. Soc.*, 1951, vol. 98, p. 425.

34. Huq, A.K.M.S., and Makrides, A.C., *J. Electrochem. Soc.*, 1965, vol. 112, p. 756.

35. Hall, S.B., Khudaish, E.A., and Hart. A.L., *Electrochim. Acta*, 1998, vol. 43, p. 579.

36. Katsounaros, I., Schneider, W.B., Meier, J.C., Benedikt, U., Biedermann, P.U., Auer, A.A., and Mayrhofer, K.J.J., *Phys. Chem. Chem. Phys.*, 2012, vol. 14, p. 7384.

37. Noël, J.M., Latus, A., Lagrost, C., Volanschi, E., and Hapiot, P., *J. Am. Chem. Soc.*, 2012, vol. 134, p. 2835.

38. Gómez–Marín, A.M., Schouten, K.J.P., Koper, M.T.M., and Feliu, J.M., *Electrochem. Commun.*, 2012, vol. 22, p. 153.

39. Katsounaros, I., Schneider, W.B., Meier, J.C., Benedikt, U., Biedermann, P.U., Cuesta, A., Auer, A.A., and Mayrhofer, K.J.J., *Phys. Chem. Chem. Phys.*, 2013, vol. 15, p. 8058.

40. Sitta, E., Gómez–Marín, A.M., Aldaz, A., and Feliu, J.M., *Electrochem. Commun.*, 2013, vol. 33, p. 39.

41. Clavilier, J., Armand, D., Sun, S., and Petit, M., *J. Electroanal. Chem.*, 1986, vol. 205, p. 267.

42. Rodes, A., Herrero, E., Feliu, J.M., and Aldaz, A., *J. Chem. Soc., Faraday. Trans.*, 1996, vol. 92, p. 3769.

43. Bard, A.J., and Zoski, C.G., *Electroanalytical Chemistry. A series of advances*. vol. 24. Chapter 2. Korzeniewsky, C., Climent, V., and Feliu. J.M., *Electrochemistry at Platinum Single Crystal Electrodes.* CRC Press, 2012, p. 75.

44. Martínez-Hincapié, R., Sebastián-Pascual, P., Climent, V., and Feliu, J.M., *Electrochem. Commun.*, 2015, vol. 58, p. 62.

45. Angerstein-Kozlowska, H., Conway, B. E., Hamelin, A., and Stoicoviciu, L., *J. Electroanal. Chem.*, 1987, vol. 228, p. 429.

46. Clavilier, J., and Huong, C.N.V., *J. Electroanal. Chem.*, 1977, vol. 80, p. 101.

47. Hamelin, A., *J. Electroanal. Chem.*, 1982, vol. 138, p. 395.

48. Hamelin, A., Borkowska, Z., and Stafiej, J., *J. Electroanal. Chem.*, 1985, vol. 189, p. 85.

49. Orlik, M., and Galus, Z., *Electrochemistry of Gold, in: Encyclopedia of Electrochemistry*, Wiley-Vch, 2007, p. 839.

50. Lachenwitzer, A., Li, N., and Lipkowski, J., *J. Electroanal. Chem.*, 2002, vol. 532, p. 85.

51. Nart, F.C., Iwasita, T., and Weber, M., *Electrochim. Acta*, 1994, vol. 39, p. 961.

52. Cahan, D., and Villullas, H.M., *J. Electroanal. Chem.*, 1991, vol. 307, p. 263.

53. Sotto, M., *J. Electroanal. Chem.*, 1976, vol. 69, p. 229.

54. Angerstein-Kozlowska, H., Conway, B.E., Hamelin, A., and Stoicoviciu, L., *Electrochim. Acta.*, 1986, vol. 31, p. 1051.

55. Kolb, D.M., and Schneider, J., *Electrochim. Acta*, 1986, vol. 31, p. 929.

56. Ferro, C.M., Calandra, A.J., and Arvia, A.J., *J. Electroanal. Chem. Interfacial Electrochem.*, 1974, vol. 55, p. 291.

57. Sotto, M., *J. Electroanal. Chem.*, 1976, vol. 72, p. 287.

58. Nieto, F.J.R., Andreasen, G., Martins, M.E., Castez, F., Salvarezza, R.C., and Arvia, A.J., *J. Phys. Chem. B*, 2003, vol. 107, p. 11452.

59. Pasquale, M.A., Nieto, F.J.R., and Arvia, A.J., *Surf. Rev. Lett.*, 2008, vol. 15, p. 847.

60. Zhumaev, U., Rudnev, A.V., Li, J.-F., Kuzume, A., Vu, T.-H., and Wandlowski, T., *Electrochim. Acta*, 2013, vol. 112, p. 853.

61. Itaya, K., Sugawara, S., Sashikata, K., and Furuya, N., *J. Vacuum Sci. & Tech. A: Vacuum Surf. Films*, 1990, vol. 8, p. 515.

62. Kondo, T., Morita, J., Hanaoka, K., Takakusagi, S., Tamura, K., Takahasi, M., Mizuki, J.I., and Uosaki, K., *J. Phys. Chem. C*, 2007, vol. 111, p. 13197.

63. Sotto, M., *J. Electroanal. Chem.*, 1976, vol. 70, p. 291.

64. Bard, A.J., and Faulkner, L.R., *Electrochemical Methods: Fundamentals and Applications*, 2nd ed.; New York, John Wiley and Sons, 2001.

65. Zhumaev, U.E., Lai, A.S., Pobelov, I.V., Kuzume, A., Rudnev, A.V., and Wandlowski, T., *Electrochim. Acta*, 2014, vol. 146, p. 112.

66. Hribar, B., Southall, N.T., Vlachy, V., and Dill, K.A., *J. Am. Chem. Soc.*, 2002, vol. 124, p. 12302.

67. Garcia-Araez, N., Rodriguez, P., Bakker, H.J., and Koper, M.T.M., *J. Phys. Chem. C*, 2012, vol. 116, p. 4786.

68. Berná, A., Climent, V., and Feliu, J.M., *Electrochem. Commun.*, 2007, vol. 9, p. 2789.

69. Vesovic, V., Anastasijevic, N., and Adzic, R.R., *J. Electroanal. Chem.*, 1987, vol. 218, p. 53.

70. Roberts, J.G., Voinov, M.A., Schmidt, A.C., Smirnova, T.I., and Sombers, L.A., *J. Am. Chem. Soc.*, 2016, vol. 138, p. 2516.

71. Li, X., Heryadi, D., and Gewirth, A.A., *Langmuir*, 2005, vol. 21, p. 9251.

72. Ataka, K., Yotsuyanagi, T., and Osawa, M., *J. Phys. Chem. B*, 1996, vol. 100, p. 10664.

73. Ataka, K., and Osawa, M., *Langmuir*, 1998, vol. 14, p. 951.

74. Sitta, E., and Feliu, J.M., *ChemElectroChem*, 2014, vol. 1, p. 55.

Figure captions

Figure 1: Cyclic voltammograms (second cycle) of Au(111), Au(100) and Au(110) electrodes in Ar-saturated, 0.1 M $HClO_4$, pH = 1.2, (thin line) and 0.1 M NaF/$HClO_4$, pH = 4.1, (thick line). Scan rate 0.05 V s^{-1}. Insets: Enlarged view in the potential region before the surface oxidation takes place.

Figure 2: Hydrogen peroxide reduction and oxidation reactions (HPROR) in quiescent, Ar-saturated 0.1 M $HClO_4$ + 1 mM H_2O_2 solutions for Au basal planes (thick lines). Blank *j-E* profiles for each plane are also given in figures (thin lines). For the sake of comparison, Figure (D) gives superimposed current profiles for all three planes. Scan rate 0.05 V s^{-1}.

Figure 3: Reduction of hydrogen peroxide in Ar-saturated, 0.1 M $HClO_4$, pH = 1.2, (thick lines) and 0.1 M NaF/$HClO_4$, pH = 4.1 (thin lines), + 1 mM H_2O_2 solutions on Au basal planes at 400, 900, 1600 and 2500 rpm (increasing currents). Scan rate 0.05 V s^{-1}.

Figure 4: Specific activity and Tafel slopes for the reduction of hydrogen peroxide in Ar-saturated, 0.1 M $HClO_4$, pH = 1.2, (thin lines) and 0.1 M NaF/$HClO_4$, pH = 4.1, (thick lines) + 1 mM H_2O_2 solutions, calculated by employing Eqn. (10). Scan rate 0.05 V s^{-1}. Dotted lines correspond to j_k calculated by Eqn. (7)

Figure 5: Positive (solid lines) and negative (dashed lines) voltammetric scans for the oxidation of hydrogen peroxide from 0.7 to 1.2 V in Ar-saturated, 0.1 M $HClO_4$, pH = 1.2, (thick lines) and 0.1 M NaF/$HClO_4$, pH = 4.1, (thin lines) + 1 mM H_2O_2 solutions at 400 (1), 900 (2), 1600 (3) and 2500 rpm (4). Scan rate 0.05 V s^{-1}.

Figure 6: Reaction order (m) for the oxidation of hydrogen peroxide in Ar-saturated, 0.1 M $HClO_4$, pH = 1.2, (filled symbols) and 0.1 M NaF/$HClO_4$, pH = 4.1, (empty symbols) + 1 mM H_2O_2 solutions on Au(100) (A), Au(110) (B) and Au(111) (C) at different potentials.

Figure 7: Specific activity and Tafel slopes for the oxidation of hydrogen peroxide in Ar-saturated, 0.1 M $HClO_4$, pH = 1.2, (thin lines) and 0.1 M NaF/$HClO_4$, pH = 4.1, (thick lines) + 1 mM H_2O_2 solutions, calculated by employing Eqn. (10). Scan rate 0.05 V s^{-1}. Dotted lines correspond to j_k calculated by Eqn. (7).

Figure 8: Oxidation of hydrogen peroxide, from 0.7 to 1.7 V, on Au(111) (A), Au(100) (B) and Au(110) (B) in Ar-saturated, 0.1 M $HClO_4$, pH = 1.2, (left) and 0.1 M NaF/$HClO_4$, pH = 4.1, (right) + 1 mM H_2O_2 solutions at 400, 900, 1600 and 2500 rpm (increasing currents). Scan rate 0.05 V s^{-1}.

Figure 9: Hydrogen peroxide reduction and oxidation reactions, from 0.05 to two different positive potential limits, in Ar-saturated, 0.1 M $HClO_4$, pH = 1.2 + 1 mM H_2O_2 solutions at 1000 rpm. Scan rate 0.05 (solid lines) and 0.005 V s^{-1} (dashed lines).

Figure 1

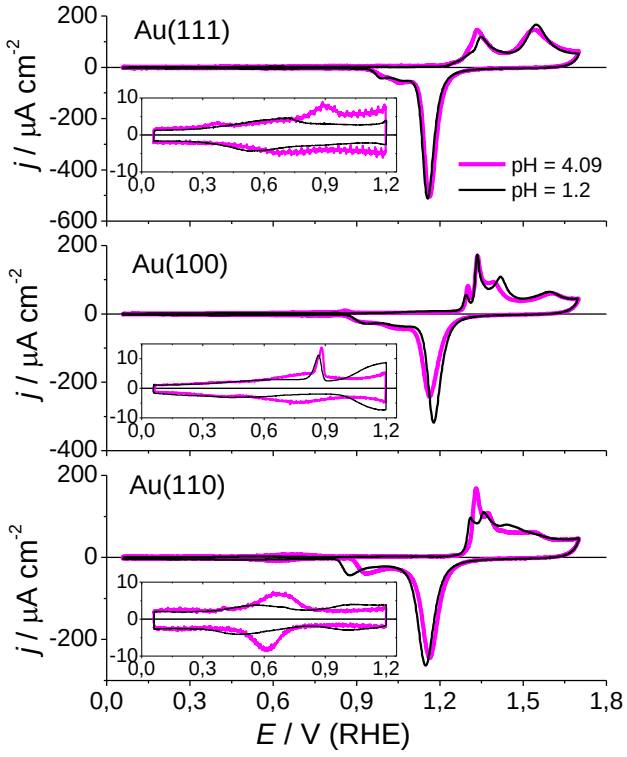

Figure 2

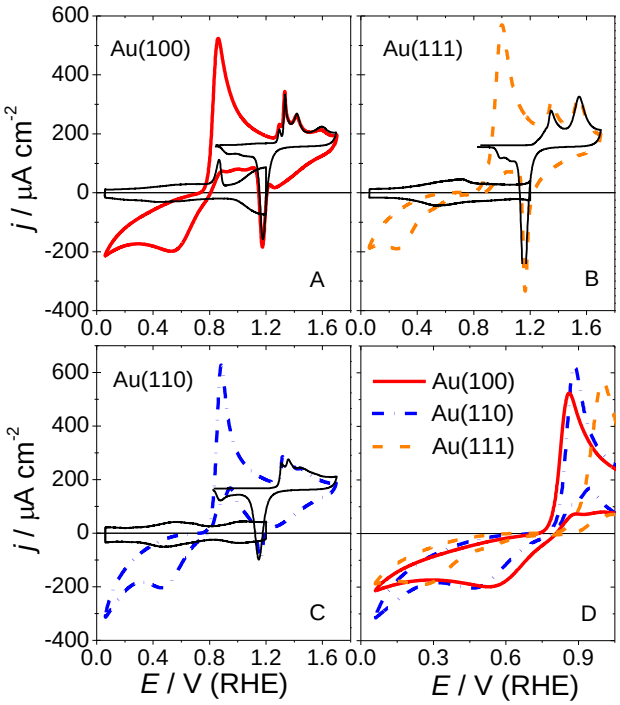

Figure 3

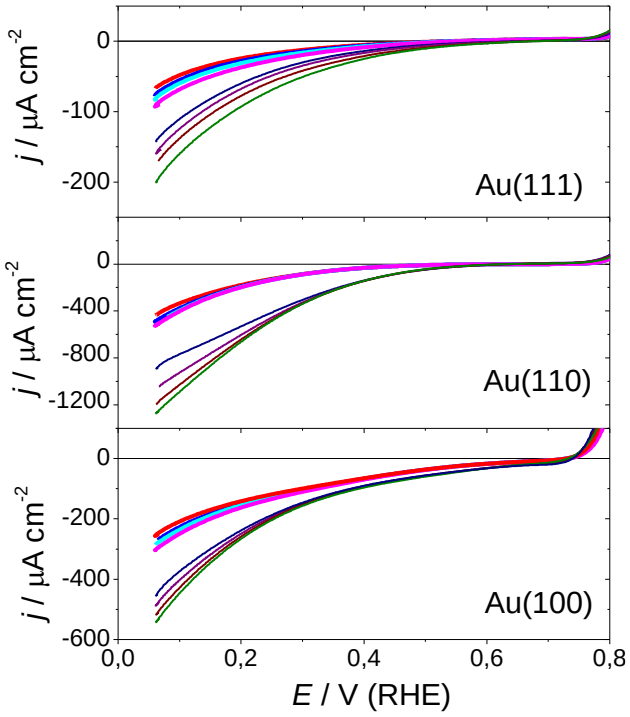

Figure 4

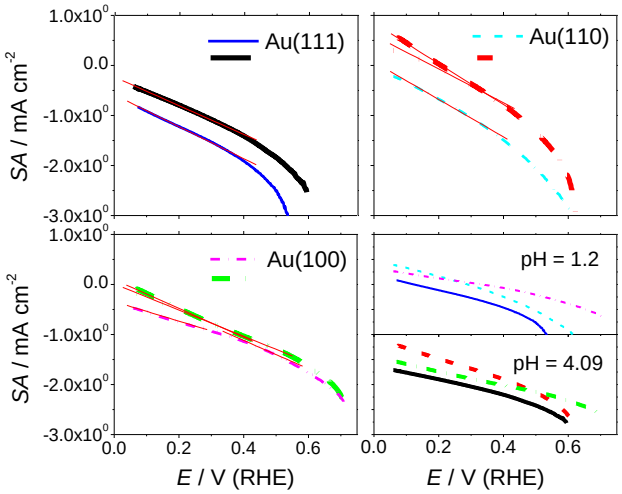

Figure 5

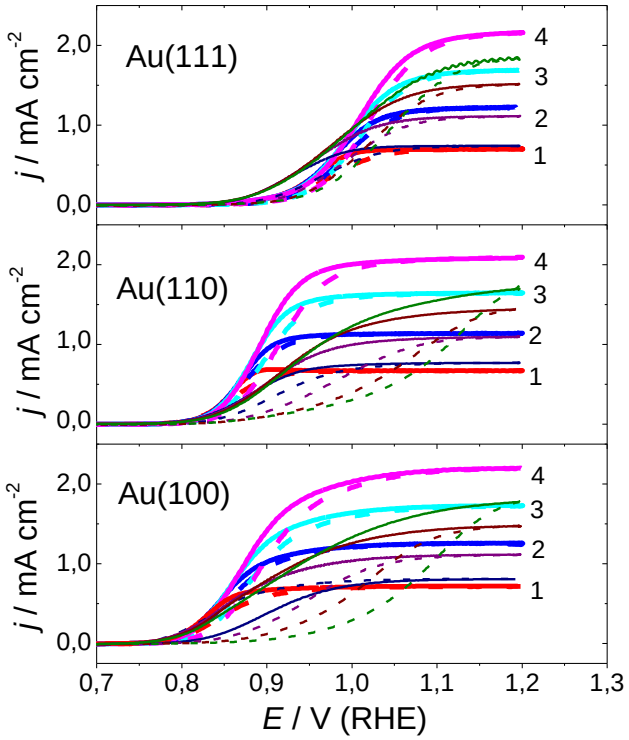

Figure 6

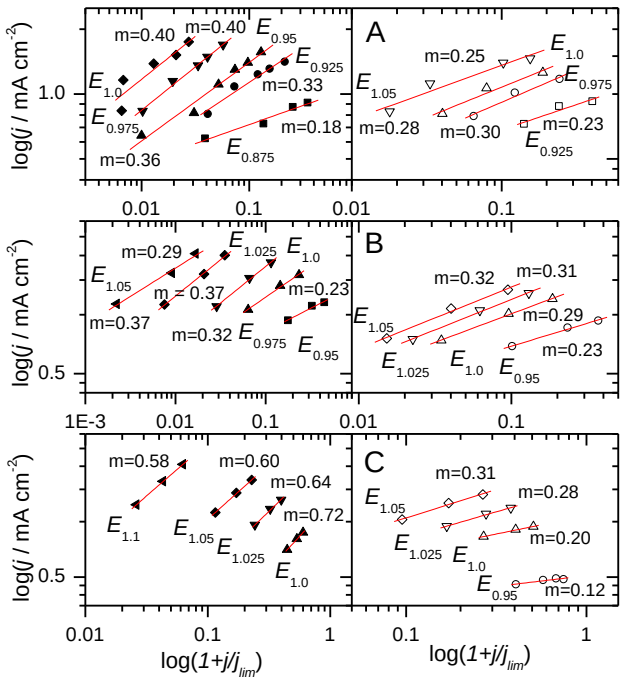

Figure 7

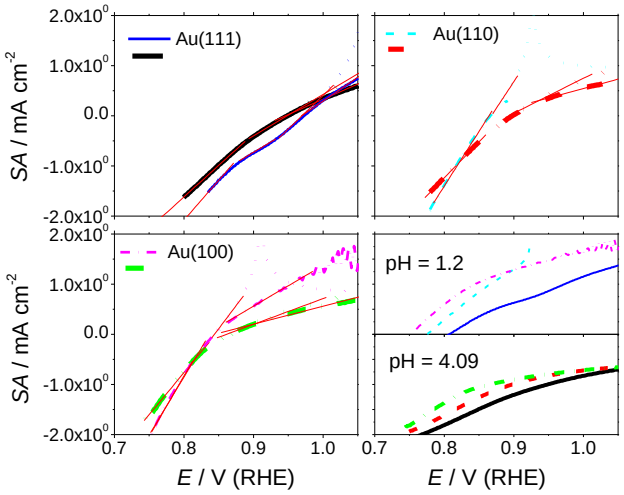

Figure 8

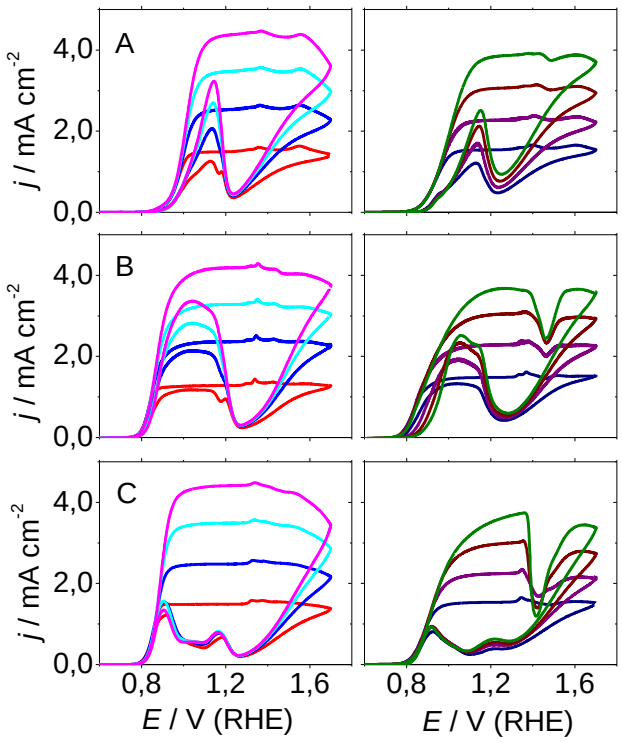

Figure 9